
Article:
Lai, Y. orcid.org/0000-0002-9987-0975, Liu, X. orcid.org/0000-0003-2419-2214, Li, Y. orcid.org/0000-0002-6570-8697 et al. (5 more authors) (2023) Investigating the fire-retardant efficiency of intumescent coatings on inclined timber: a study on application strategies and heat transfer mechanisms. Construction and Building Materials, 407. 133586. ISSN 0950-0618

https://doi.org/10.1016/j.conbuildmat.2023.133586

Construction and Building Materials 407 (2023) 133586

Contents lists available at ScienceDirect

Construction and Building Materials

journal homepage: www.elsevier.com/locate/conbuildmat

Investigating the fire-retardant efficiency of intumescent coatings on inclined timber: A study on application strategies and heat transfer mechanisms

Yufeng Lai [a], Xuanqi Liu [b,c,*], Yifan Li [d], Emilios Leonidas [e], Callum Fisk [a], Jiansheng Yang [f], Yang Zhang [g], Jon Willmott [a,*]

[a] Department of Electronic and Electrical Engineering, The University of Sheffield, Sheffield, S1 4ET, United Kingdom
[b] School of Low-Carbon Energy and Power Engineering, China University of Mining and Technology, Xuzhou 221116, China
[c] Research Center for Smart Energy, China University of Mining and Technology, Xuzhou 221116, China
[d] Department of Civil and Structural Engineering, the University of Sheffield, Sheffield S1 3JD, United Kingdom
[e] Department of Materials Science and Engineering, The University of Sheffield, Sheffield S1 3JD, United Kingdom
[f] The Electrical Engineering College, Guizhou University, Guiyang, China
[g] Department of Mechanical Engineering, The University of Sheffield, Sheffield S1 3JD, United Kingdom

ARTICLE INFO

Keywords:
Fire-retardant coating
Visualisation
Timber material
Heat transfer
Burning behaviour
Inclined angle

ABSTRACT

The impact of intumescent flame-retardant (IFR) coating location on the fire-resistance of inclined timber samples was studied using a multi-imaging system that integrated visible wavelength, short-wavelength infrared (SWIR), long-wavelength infrared (LWIR), and Schlieren techniques. Weight loss post-initial ignition was monitored using a weight scale, and a scanning electron microscope (SEM) was employed to observe the microstructure of both coated and uncoated surfaces post-burn. Samples were inclined at 30°, 45° and 60° to study the effects of inclination on fire-retardant efficiency. Four coating strategies were compared: top surface, bottom surface, one side surface, and both side surfaces, against an uncoated control. Quantitative results revealed significant reductions in burning intensity and fire spread when coating was applied to the bottom surface and both side surfaces, attributed to the inhibition of convective heat transfer from underneath the timber samples. The mechanisms of this inhibition were considered to be the termination of gas-phase combustion and impediment of pyrolysis product escape. Furthermore, the fire-retardant efficiency diminished with increasing inclination angles, especially for samples coated only on the top or one side. Conceptual models were developed to understand the mechanisms of fire-retardance and heat transfer inhibition. This work offers critical guidance for the application of fire-retardant coatings and may enhance cost efficiency in fire safety, particularly for individual elements of timber structures such as beams, columns, and frames.

1. Introduction

Modern constructions are increasingly using timber-based materials due to their advantages in sustainability and structural performance. Compared to concrete structures, timber-based structures have an outstanding advantage in reducing carbon emission throughout the building life cycle assessment [1–3]. In addition, characteristics such as being biodegradable, sustainable [4] and recyclable [5] make timber an environmentally-friendly material in the construction industry. Instead of using solid wood, engineered timber materials such as Laminated Veneer Lumber (LVL) [6], Laminated Strand Lumber (LSL) [7], and Cross Laminated Timber (CLT) [8] are mainly used; since they are more cost-effective and have better structural performance. However, due to the combustible nature of timber, the fire safety of timber constructions, especially in high-rise buildings, poses challenges to civil engineers and researchers [9,10].

In fire safety design of timber structures, the fire resistance of a building is generally defined by a certain fire exposure time while maintaining its structural integrity [11,12]. In fire involving timber structures, the exposed timber elements can contribute to the existing fuel load within the fire compartment, leading to higher peak temperatures, longer heating times, and faster fire growth rates [13,14].

* Corresponding authors.
E-mail addresses: xuanqi.liu@cumt.edu.cn (X. Liu), j.r.willmott@sheffield.ac.uk (J. Willmott).

https://doi.org/10.1016/j.conbuildmat.2023.133586
Received 10 July 2023; Received in revised form 12 September 2023; Accepted 27 September 2023
Available online 30 September 2023

Charred timber is defined to have zero strength and stiffness in fire safety design according to BS 1995-1-2 [11], since the charring process can reduce the effective cross-sectional area, thereby lowering the load-bearing capacity of the whole structure [11]. To increase the fire resistance of timber materials, the intumescent coating has been used as a passive fire protection method. Under heat exposure, the coating can swell up to 100 times its original thickness, forming a fire insulation char barrier [15]. Also, the intumescent coating has been reported to be cost-effective and environmentally friendly [15].

Researchers have conducted a wide range of tests on the intumescent coating on timber samples in laboratory-scale experiments. Lucherini et al. used different thicknesses of commercially available intumescent coating to study the burning behaviours (ignition time and temperature) and char properties (depth and swelling) on an Australian soft wood [16]. Jiang et al. quantified the temperature of the maximum rate of pyrolysis decreased with the percentage of wood treated with IFR (intumescent fire retardant), the temperature for original wood is about 325 ℃ [17]. The high efficiency and eco-friendly IFR coating has been developed from various aspects, for example the modified decanoic/palmitic eutectic mixture (DPEM) [18], different carbon sources additives [19], bio-based FRC curing agent of ammonium hydrogen phytate (AHP) [20], gibbsite/SAE-based [21] and more novel designs of the intumescent itself [20,22]. The comprehensive characterisation has been done with those designed coatings, and a compact, continuous and uniform char layer has been considered as an adequate structure for a high-efficiency coating. The existing literature provides valuable insights into the properties of different IFR coatings and the corresponding local burning behaviours, using techniques such as the gas-spray gun heating tests [20,22]. However, there are lack of understanding of fire spread mechanism, especially in the effects of IFR on the fire spread dynamics.

Large-scale experiments have been conducted for studying flame dynamics and validating the findings revealed from the laboratory-scale experiments. Zhang et al. [23] conducted a large-scale light timber frame construction (LTFC) and investigated the fire development and flame behaviours. Their results showed that the temperature of gas surrounding the timber frame played an important role in flame ejection distance and the preheating process. Self-sustained burning on timber materials required sufficient heat and preheating on the virgin materials [24]. It has been demonstrated that convection plays the primary role to sustain the burning and spread the fire on timber materials, especially for a single-element structure [24,25]. And the underneath hot flow layer was considered as the dominate source for the convective preheating [26].

Upon reviewing the available literature, several gaps in the research have been identified: 1) Although comprehensive studies have been conducted on local burning behaviours, the study of fire spread on IFR coated timber remains unexplored. 2) To the authors' knowledge, no publications have yet investigated the influence of the different coating locations on the effectiveness of fire-retardant measures. Moreover, the inclined angle of the structure can potentially impact the effectiveness of the coating. Thus, studying the effects of coating location and inclination angles carries substantial practical and theoretical significance. 3) A comprehensive visualisation system for fire safety assessment is desirable because it can enhance our understanding of the fire-retardant mechanisms and the heat transfer process.

The aim of this study was to investigate the effects of the coating location, on the fire-retardant effectiveness, on single-element timber structures, at different inclination angles. We developed a synchronised visualisation system, which includes: direct imaging (photography) to quantify charring behaviour; Schlieren imaging, which can enable visualisation of hot gas flow surrounding the burning timber; and two thermal cameras, providing quantitative results of the surface temperature. Along with a weight scale and scanning electron microscopy (SEM), the burning process of the IFR-coated timber can be comprehensively visualised and studied. The mechanisms of intumescent coating inhibition of the heat transfer have been revealed from the quantitative results. A conceptual model has also been developed.

The effectiveness of different fire-retardant coating locations is explored and presented here in literature for the first time. The insights gained in this work may provide an important framework for future design of the fire safety engineers and aid in the development of timber-substrate intumescent coatings. The outcomes of the study could also help to improve the cost efficiency of employing fire-retardant coatings, especially for single-element structures such as beams, columns and frames.

2. Methodology

2.1. Experimental arrangement

The experiment setup is illustrated in Fig. 1. Four cameras were used to synchronously monitor the fire spread process, the imaging and trigger system are shown in Fig. 1(a). Each imaging method can provide insights from different aspects of the fire development. The mechanisms of fire-retardance can be revealed by combining these aspects, as shown in the example images in Fig. 1 (c). The direct images, using a colour camera, record the whole burning process, and the burning behaviours (charring rate and maximum charring distance) can be obtained during post-processing. The Schlieren imaging system enabled the visualisation of the hot gas flow field surrounding the burning wood. The hot flow is crucial in the convective heat transfer of the fire spread [24]. The Schlieren images were captured by a grey-scale high-speed camera. Two thermal cameras: long-wavelength infrared (LWIR) and short-wavelength infrared (SWIR), were used for monitoring the side surface temperature, temporally and spatially. The mechanisms of heat transfer inhibition can be revealed through the combination of thermal and Schlieren imaging.

The test zone is depicted in Fig. 1 (b). The samples were 9.5 mm × 9.5 mm × 240 mm natural oak wooden cuboids. All samples were pre-dried for 12 h at 100 °C, in a furnace, ensuring the consistency of moisture content. An adjustable holder was used to secure the samples and set the incline angles at 30°, 45°, 60°. The holder and the sample were placed on a weight scale allowing weight loss during the burning process to be measured. The samples were inclined because the fire spread changes as a function of inclination [27]; indeed, the inclined timber structure generally accelerates the fire spread and can cause more serious loss [28]. A premixed methane-air flame was used as an ignition source with a methane flowrate of 0.35 L/min and 0.9 L/min for air. A 40 mm distance was maintained between the sample and the burner. All samples were ignited for 20 s before turning off the burner. The first 80 mm length from the ignition point was set as the self-sustained region allowing the fire development after piloted ignition, shown in Fig. 1 (b).

A commercially available thin intumescent (Model 92-ESVFR, Lifeline Fire Prevention Ltd) was applied to different surfaces beyond the self-sustained region (80 mm), as shown in Fig. 1 (d). The coating is an aqueous (emulsion) acrylic polymer system which is widely used for timber materials because the easy application and good adhesion to the wood surface. However, potential hazards can be raised such as environmental impact and toxicity. The IFR coating was applied by brushing the surface evenly, with the uncoated surface covered for protection. The commercially available intumescent coating was ideal for studying the burning behaviours of timber because their widespread adoption and representativeness [16]. The sample without any coating (labelled as: None) was used as a control. Subsequently, the top surface (labelled as: Top), bottom surface (labelled as: Bottom), one side surface (labelled as: One side) and both side surfaces (labelled as: Both sides) were treated with the intumescent, to investigate the effectiveness of the fire-retardant under different coating strategies and to study the mechanisms of fire inhibition in timber fires.

The surfaces of both coated and uncoated samples were analysed

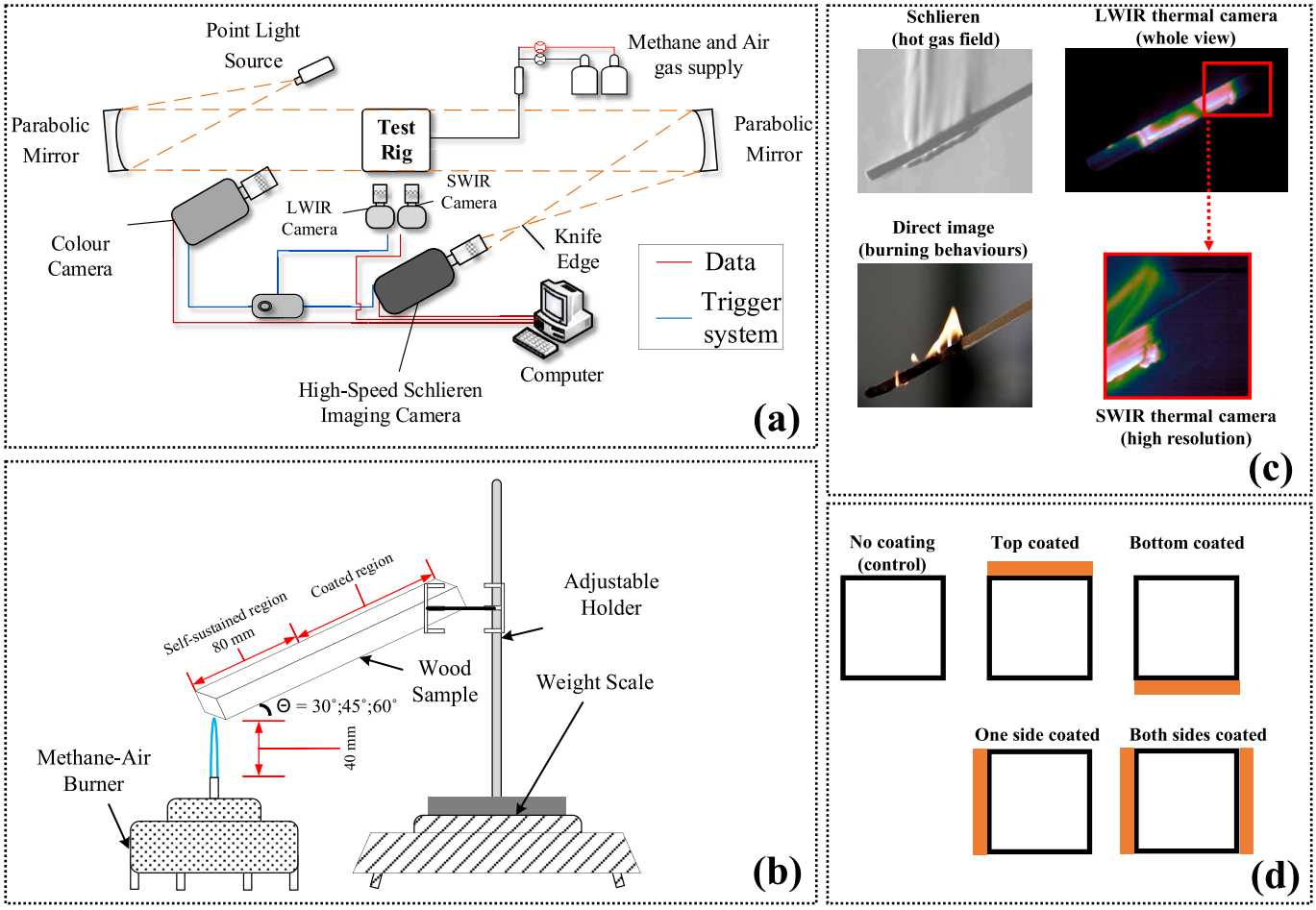

Fig. 1. The experimental arrangement. (a): Imaging system setup. (b): Test rig illustration. (c): Example images of the synchronised imaging system. (d): Illustration of the different coated surfaces (cross-section view)).

post-experiments using the FEI Inspect F SEM to perform scanning electron microscopy (SEM), at an acceleration voltage of 5 kV and a spot size of 3 nm. The SEM images enabled us to present the differences in the microstructure of the surfaces. We present these with and without the coating, allowing a detailed investigation of flammable gas escape in conjunction with Schlieren imaging.

2.2. Burning behaviours

The overall burning behaviours were assessed from three key perspectives; weight loss, which correlates to the burning rate of the natural timber; charring rate and the maximum charring distance in the coated region, which reflected the temporal and spatial progression of the fire respectively. The maximum charring distance was considered only for the bottom and both sides coating strategies because the fire was able to spread throughout the sample in other coating surface cases. Timber materials have the natural of the inhomogeneous internal structure which resulted in the deviation from the results. Therefore, each test was repeated for five times, to ensure repeatability. The time evolution of weight loss is presented as the most representative result, while the charring rate and charring distance, obtained from direct imaging, are averaged and the repeatability of the tests are well presented with the calculated standard deviation.

The weight loss, as recorded by the scale, was normalised based on the initial weight of the samples, for a more direct comparison among the different test groups. Results were presented from the moment the initial ignition was turned off, to either the extinguishment of the fire, or the point at which the fire reached the farthest end of the samples.

Charring rates and the maximum charring distance in the direction of fire spread were quantified using the direct images. These were calculated based on the distance that the leading carbon black travelled, starting from the coated region, until the fire was either extinguished (in the cases of Bottom and Both sides) or reached the farthest end of the samples (for None, Top, and One side), and the time this process took. The results were then averaged across repeated tests and their respective standard deviations are also presented.

2.3. Temperature measurement

The temperature profile of the side surface can be used to visualise the effectiveness of each coating strategy, in inhibiting heat transfer thereby aiding the investigation into the mechanisms of fire retardation. Two infrared cameras were employed in this study: LWIR camera (PyrOptik, model LW640) and InGaAs SWIR camera (PyrOptik, model NIRIN640), to monitor the side surface temperature of the samples after initial radiance calibration.

The LWIR camera, operating at a fixed framerate of 9 Hz and a resolution of 640 × 512 pixels, was sensitive to the long-wavelength infrared range (7.5 μm – 13.5 μm). This sensitivity enabled the camera to detect radiation emitted from low temperature surfaces. The calibration process was similar to the work of Lai et al. [29]. A blackbody furnace (emissivity ~ 0.99) was used as the calibration source across a temperature range of 50 °C to 650 °C, with calibration points taken at 50 °C increments. Fig. 2 (a) shows the calibration curve and measured uncertainty of LWIR camera. The uncertainty (residuals) was quantified as the difference between the furnace temperature and the calculated

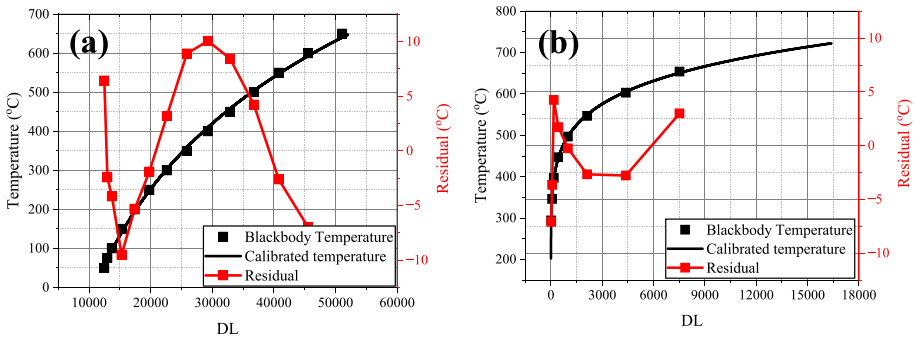

Fig. 2. Calibration and uncertainty of measured temperature: (a) LWIR camera and (b) InGaAs SWIR camera.

temperature. The results show the maximum residual was less than 10 °C which provides adequate performance for the purposes of this research.

The InGaAs SWIR camera equipped with a 100 mm focus lens can provide a narrower field-of-view (FOV) but more detailed imaging than LWIR measurements. The spectral sensitivity was restricted in the range of 1490 nm – 1502 nm by a band pass filter (Thorlabs, FBH1490-12) to obtain an accurate temperature reading from 250 °C to 700 °C. The calibration was based on Planck's Law [29], 100 images were captured and averaged with a blackbody furnace (emissivity ~ 0.99) between 250 °C and 700 °C, at increments of 50 °C. The offset from zero digital-logic-levels, under unilluminated conditions, was determined by averaging 100 images with the lens covered. The calibrated temperature curve is shown in Fig. 2 (b). It was found that the measurement uncertainty of the InGaAs camera was less than 5 °C across the specified temperature range of 300 °C to 700 °C.

The radiance captured by both thermal cameras was corrected by the estimated emissivity of burnt wood. A fixed emissivity of 0.95 was employed in this work based on the literature [26,30].

The LWIR camera was used to provide temporal temperature results because of its wide FOV and large dynamic range (50 °C to 650 °C). A region-of-interest (ROI) measuring 20 mm in length within the coated region was selected for analysis, shown in Fig. 3 (a). This length was determined based on the average charring distance observed in the coated region of bottom-coated samples. The surface temperature was averaged for quantitatively indicating the mean temperature change as fire spread into the coated region.

The SWIR camera, with its narrower FOV and more precise temperature readings ranging from 250 °C to 700 °C, was aptly suited for presenting the spatial distribution of temperature. To investigate the mechanisms of heat transfer inhibition with different coating strategies, the pyrolysis length and the mean temperature of the pyrolysis zone were measured as a function of the distance to the bottom surface, shown in Fig. 3 (b). The pyrolysis zone was defined as the pixels whose temperature was higher than 300 °C. This threshold was chosen based on the understanding that rapid pyrolysis of wooden fuels typically occurs above 300 °C [31,32], effectively delineating the region undergoing active flaming combustion. The size of each pixel of the camera covered was pre-calibrated, enabling the calculation of the pyrolysis length from the thermal images. Results were presented at 20 s, 40 s and 60 s to illustrate the temporal evolution of the pyrolysis zone under different coating strategies.

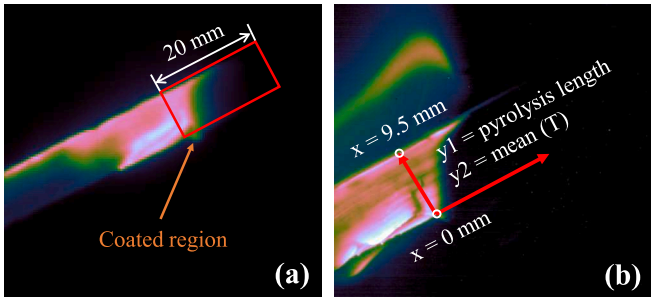

Fig. 3. Illustration of the region of interest (ROI). (a): The temporal mean temperature of LWIR camera. (b): The spatial distributions of the pyrolysis zone in the coated region of InGaAs SWIR camera.

3. Results and discussions

3.1. Burning behaviours

Fig. 4 shows direct photographic images of the wooden samples inclined at 30°, capturing the moment when fire spread to the coated region and moved throughout the sample (or until extinguishment). These images evidenced that different coating strategies can significantly influence the burning behaviours of the sample, which in turn impacts the effectiveness of fire-retardant. Specifically, with top surface coating, the fire continues to spread throughout the sample, albeit with a somewhat weakened top flame (compared to the 'None'). With one side surface coating, the fire similarly propagates throughout the sample, but only partially chars the coated surface. The strategies of coating the bottom and both sides effectively inhibit fire spread. In the bottom-coated sample, the fire tends to spread from the top, while in the sample coated on both sides, the fire primarily spreads near the bottom.

The effectiveness of the fire-retardant can be assessed by the quantifying burning behaviours. Fig. 5 presents the normalised weight loss for different coating strategies when the sample was inclined at various angles. The weight loss in the self-sustained region remained consistent at each inclined angle. However, the weight loss rate became larger when the inclined angle gets steeper. Similar findings were revealed by Gollner et al. [33]. This was due to the inclined surface, which effectively enhanced the heat convection to the virgin wood. As a result, fire spreads into the coated region faster on samples with a larger inclined angle.

The decreased weight loss rate in the coated region indicates the effective retardant of fire. The effectiveness of the coating strategies was ranked as follows: Both sides > Bottom > One side > Top (30°) and Both sides > Bottom > Top > One side (45° and 60°). The bottom and both sides coating strategies were successful in stopping the spread of the fire, with limited weight loss found in the coated region. Top and one side coating strategies provided a considerable inhibition of combustion when the sample was inclined at 30°, as the weight loss rates significantly decreased. This can also be seen in Fig. 4, which displays weakened flaming combustion. However, with increased inclination, the effectiveness of fire retardation decreased, as the weight loss rates came close to those of the control group (refer to Fig. 5 (b) and (c)).

To further investigate the effects of the inclined angles on the fire-retardant effectiveness, Fig. 6 compares the weight loss rates at different inclinations. Fig. 6 (a), as a control group, represents the weight loss rate under self-sustained burning. As previously discussed,

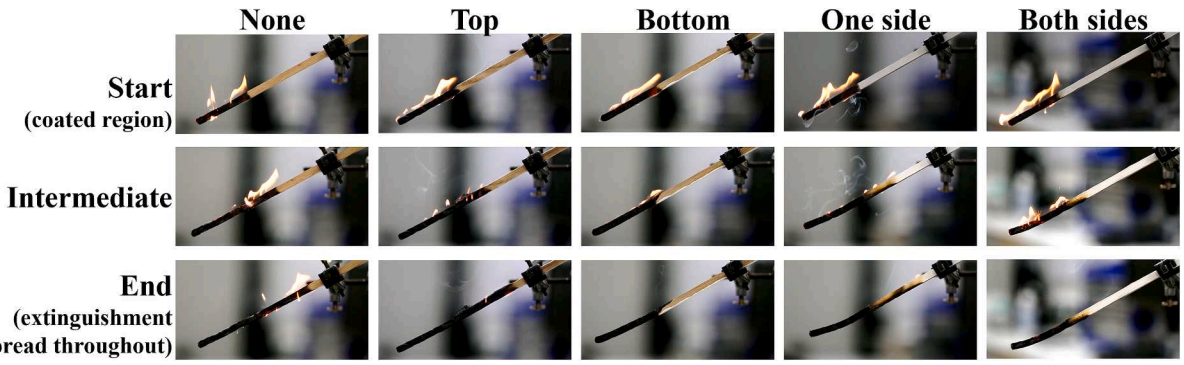

Fig. 4. Direct images of fire spread to the coated region (start), intermediate and to the end of the sample (or extinguishment) at 30° inclined angle.

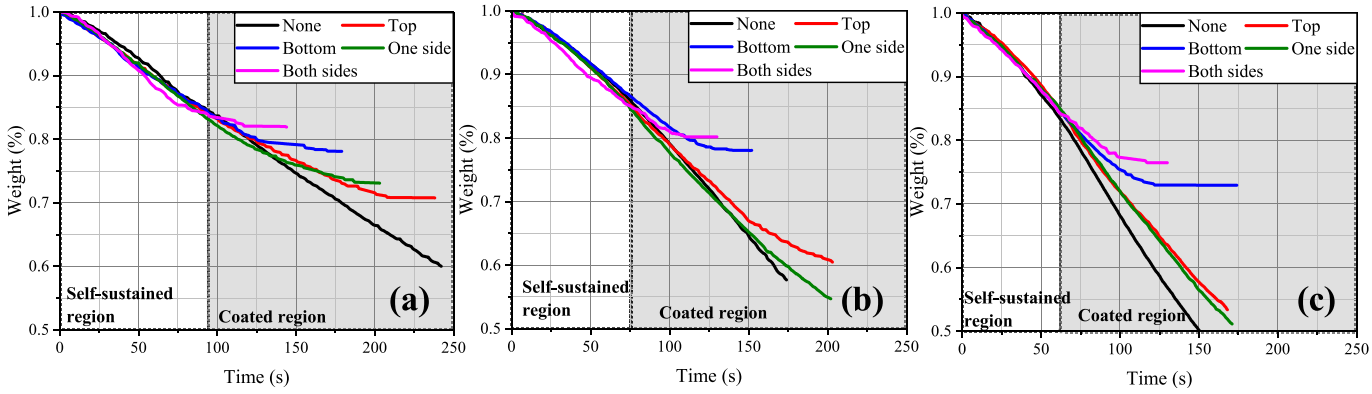

Fig. 5. Time evolution of weight loss with different coated strategies. (a) Sample inclined at 30 degrees. (b) Sample inclined at 45 degrees. (c) Sample inclined at 60 degrees.

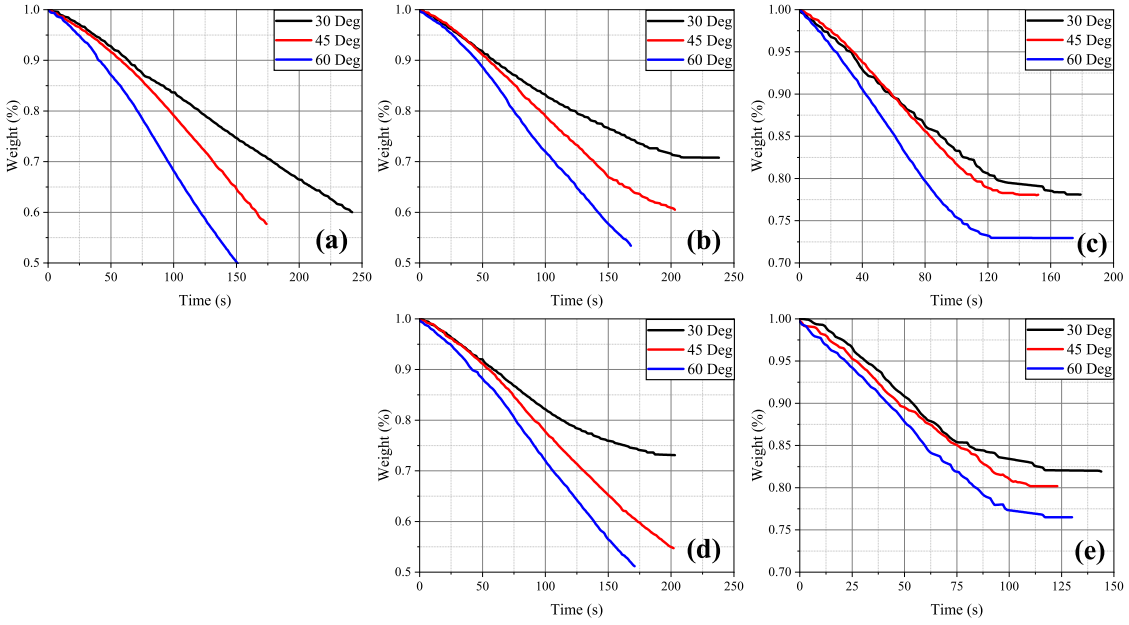

Fig. 6. Weight loss evolution compared between different inclined angles with different coating strategies. (a) No coating applied. (b) Top surface coated (c) Bottom surface coated. (d) One side surface coated. (e) Both side surfaces coated.

the more efficient heat transfer to the virgin wood facilitated the fire spread and took a larger volume of wood into the thermal pyrolysis [24]. In general, the fire-retardant effectiveness of all coating strategies decreased with a larger inclination angle, which was due to the increased flame attachment length [27] and more effective heat convection [24]. In detail, the top and one side coatings almost lost efficacy when the angle was larger than 45°. The effectiveness of the bottom and both sides coating decreased slightly under a larger inclination, but the fire could be stopped within a short period.

Fig. 7 shows the char propagating behaviours in the coated region

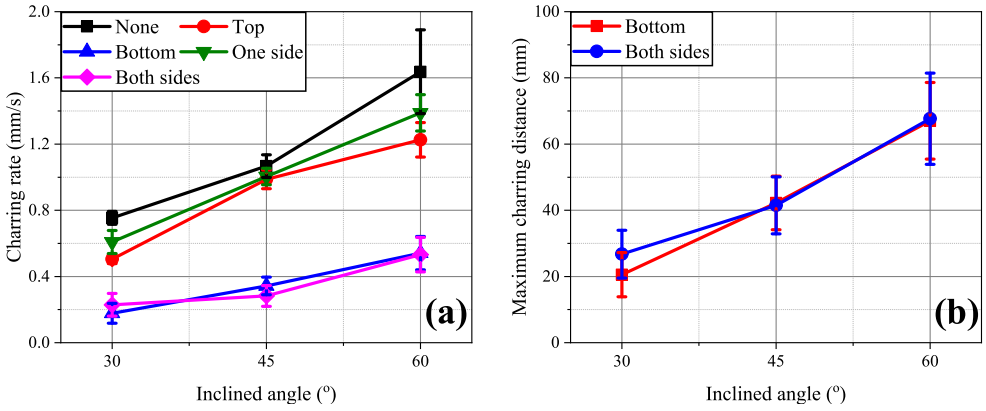

Fig. 7. Charring behaviours in the coated region (D > 80 mm). (a): Charring rate on the direction of fire spread of different coated strategies. (b): Charring distance before extinguishment of bottom and both sides coated (Fire spread throughout the sample in other cases).

under various coating strategies and inclined angles. The charring rate increased with the larger inclined angles (Fig. 7 (a)), which aligned with both the weight loss rate findings and existing literature [24,33]. Regarding the coating strategies, the top and one side coating had insignificant inhibitory effects on the charring rate compared to the control group. In contrast, the bottom and both sides coating impeded the charring rate. The charring of a timber material requires a sufficient temperature for thermal pyrolysis, and a higher charring rate is associated with effective heat transfer to virgin materials [31]. A coating on the bottom surface obstructs the spread of hot gas flow beneath the sample, which is crucial in preheating the virgin wood [34]. Coating at both side surfaces inhibits the convective heat transfer to the upper surface of the timber, leading to less material being involved in thermal pyrolysis.

Fig. 7 (b) shows the maximum charring distance of the bottom and both sides coating strategies. These two coating strategies have similar charring distance but char was produced on different surfaces, as shown in Fig. 4. For the bottom coated sample, charring tended to occur on the top surface. This was because the radiative heat transfer from the flame on the top side becomes the primary source of heat flux when the preheating from underneath was inhibited. On the other hand, for the sample coated on both sides, the flow underneath can preheat the virgin wood on the bottom side. However, the IFR coating on both sides obstructed natural convection, which further supressed the initiation of combustion on the upper surface. Regarding the inclination angles, a larger inclination increases the area that can be preheated by the convection from underneath, which means that char can travel further under a larger inclined angle.

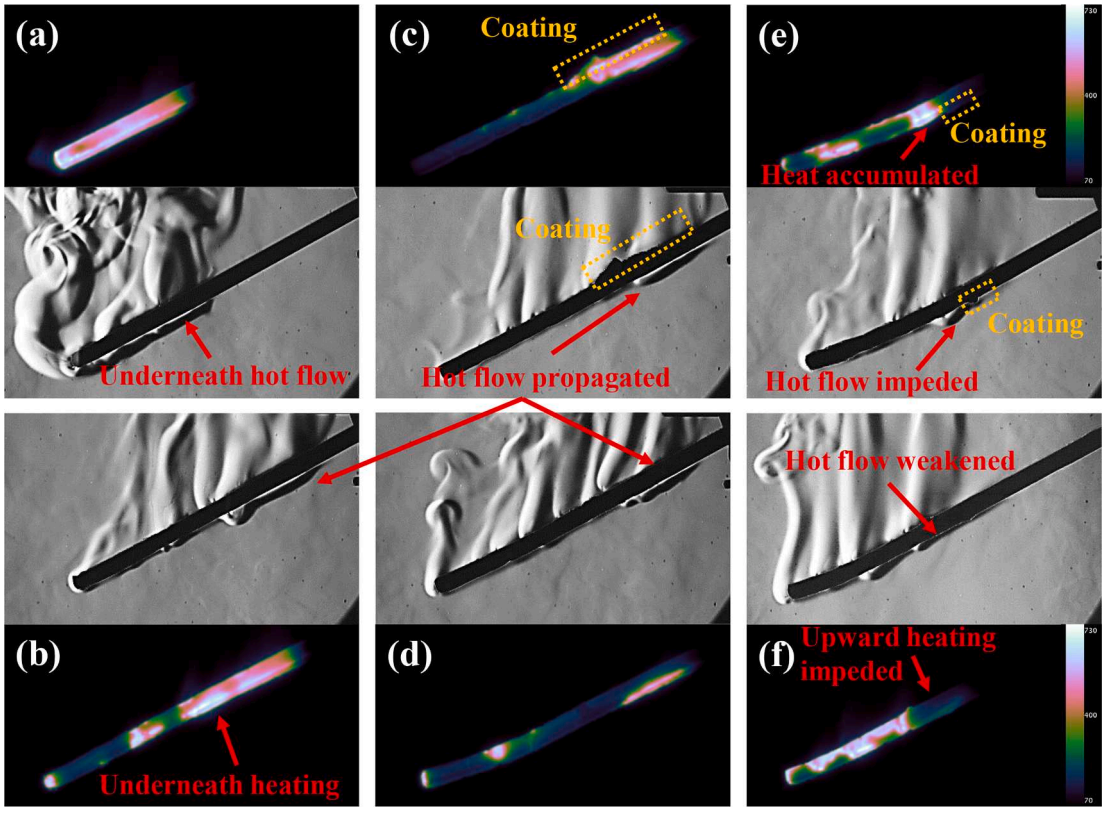

Fig. 8. Hot gas flow field presented by schlieren imaging of different test cases and the corresponding thermal images. (a): Burning at self-sustained region. (b – f) burning at coating region; (b): No coating applied. (c): Top surface coated. (d): One side surface coated. (e): Bottom surface coated. (f):Both side surfaces coated.

3.2. Hot gas flow field

Schlieren imaging can capture minor changes of the gas density and has been used for investigating the hot gas flow during the combustion previously [26]. Fig. 8 illustrates typical Schlieren images of each coating strategy, along with their synchronised thermal images. A pronounced hot flow is observed underneath the timber sample in its self-sustained state (Fig. 8 (a)). This hot gas flow, composed of the burnt gases from the combustion of timber and the flammable gases generated from the thermal pyrolysis [24], is crucial for preheating the virgin wood and supplying the gas-phase fuel for the flaming combustion. This hot gas flow invariably leads the fire spread (Fig. 8 (b)).

The underneath flow appeared slightly thinner and shorter with top and one side coating (Fig. 8(c) and (d)), but was still able to spread throughout the samples. This can be attributed to the fact that fewer materials were involved in the pyrolysis, leading to fewer burnt gases and flammable gases being generated. It is found from the thermal images of one side coating (Fig. 8 (d)) that the heat was concentrated near the bottom of the sample, suggesting the intumescent coating on the side surface effectively obstructed the convective heat transfer from underneath the sample. As a comparison, in the top surface coated sample (Fig. 8(c)), heat can be transferred into the upper region, resulting in a larger area with high temperature.

Conversely, the propagation of the underneath hot flow was limited in the bottom and both sides coated samples (Fig. 8 (e) and (f)). As observed in Fig. 8 (e), the heat accumulated in the region before the intumescent coating, a consequence of the hot flow being impeded by the bottom surface coating. A portion of the wood preheated near the upper surface was heated by the flame radiation [31]. However, the heat cannot transfer downward because of the buoyancy [32], resulting in only a limited length of the lower surface being heated. This forms the mechanism underpinning the high performance of the fire-retardant using the bottom coating strategy.

The underneath flow was weakened in both-sides-coated sample (Fig. 8 (f)) and cannot propagate over a long distance. The preheating region was found nearer the lower surface, as opposed to the upper surface in the bottom surface coated sample (Fig. 8 (e)). This was because the underneath flow in both-sides-coated sample could still propagate and preheat the virgin timber. However, upward convective heat transfer was effectively inhibited due to both sides being coated. Given the low thermal conductivity of timber [35], heat was isolated between the upper and lower surfaces. With insufficient heat and flammable gases provided from below, the flaming combustion on the upper side could not be sustained. As a result, the hot flow became weakened due to the inhibition of global combustion, subsequently obstructing the spread of fire.

3.3. Temperature distributions

The hot flow gas flow markedly influenced the surface temperature of the samples. The measuring of surface temperature offered essential insights into burning behaviours, regions under thermal pyrolysis, and preheating stages. Typically, timber materials initiate rapid thermal pyrolysis at temperatures around 300 °C, producing volatiles that subsequently triggers spontaneous flaming combustion [36]. On the other hand, when the samples have surface temperature of samples ranging from 200 − 300 °C, pyrolysis is more likely to produce solid products, such as carbon char [37,38]. Thermal imaging has emerged as a promising tool for acquiring the temperature distribution across the timber surface and identifying parts of the structure that have undergone decomposition [39].

Fig. 9 shows the average temperature of the ROI in the coated region, considering different coating strategies and inclination angles. It is observable that the surface temperature of uncoated samples was generally the highest and sustained for longer periods of time at high temperatures (T > 300 °C). This phenomenon was most conspicuous when the sample was inclined at 30° (Fig. 9 (a)), where only the top-coated sample exhibited a comparably high surface temperature but lasted a short period of time, which was attributed to paucity of timber in the upper region undergoing pyrolysis and the reduced radiation from the flame. The surface temperature of the bottom and both sides coated samples were the lowest (~200 °C), indicating that charring combustion predominantly occurred rather than gas-phase combustion.

The surface temperature increased with the larger incline angles, as shown in Fig. 9 (b) and (c). In other words, the effectiveness of the intumescent coating diminished with the increasing inclinations. This phenomenon can be attributed to the longer length of the underneath hot flow and the flame attachment on the upper surface, resulting in a more extensive thermal decomposition of the materials [27]. Additionally, the increased angles also enhanced the efficacy of heat transfer to the virgin timber via both convection and flame radiation. It was observed that the top and one-side coating strategies nearly lost their effectiveness when the angle was larger than 45°, since no significant difference in surface temperature and sustaining duration can be found between them and control group. In contrast, for the bottom and both-sides coated samples, the surface temperature remained suppressed compared to the uncoated sample, even though their effectiveness decreased with the larger angles.

In contrast to the side coating (either on one side or both sides), which hindered the convective heat transfer from the underlying hot flow to the upper surface, the top and bottom coating functioned differently by directly inhibiting the heat source from the respective top and bottom surfaces. The structural integrity of timber significantly diminishes once rapid thermal pyrolysis is initiated, given that charred wood possesses inferior mechanical properties compared to the original

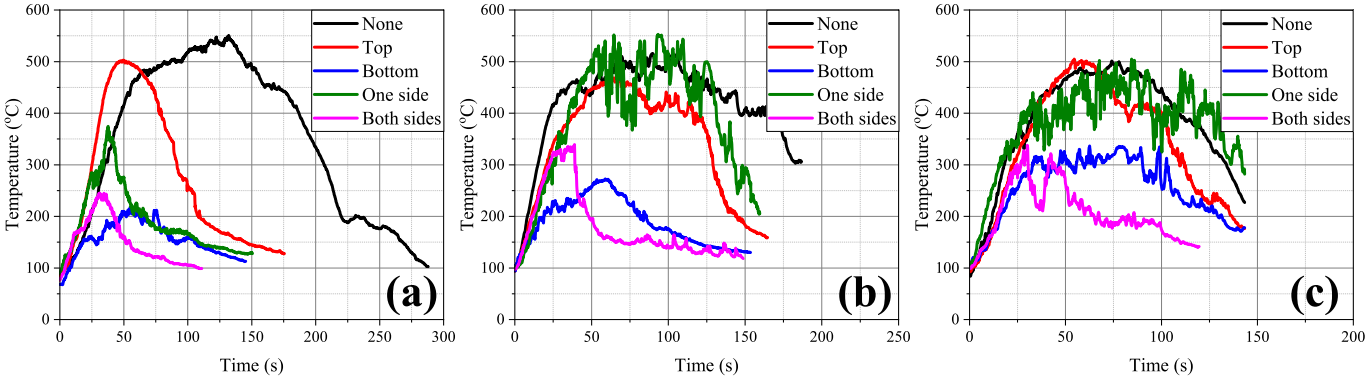

Fig. 9. Averaged side surface temperature of the ROI in the coated region of different coated strategies and inclined angles. (a) Sample inclined at 30 degrees. (b) Sample inclined at 45 degrees. And (c) sample inclined at 60 degrees.

material [40]. Fig. 10 shows the length of the rapid pyrolysis zone (T > 300 °C) in relation to the distance to the bottom surface (as illustrated in Fig. 3 (b)), along with its mean temperature at t = 20 s, 40 s and 60 s.

Fig. 10 (a) reveals that the primary pyrolysis zone in the bottom-coated sample was located near the top surface (x = 4 – 9.5 mm), while the timber had a restricted pyrolysis length near the bottom surface. This was attributed to the intumescent coating obstructing the propagation of the hot flow underneath, meaning the lower surface of the timber was hardly heated due to the lack of convective preheating from a sufficient hot flow. The timber at the upper surface could undergo thermal pyrolysis as a result of flame radiation. However, due to the low thermal conductivity of timber, heat could not effectively transfer from the upper surface to the lower, leading to a shorter burning lifetime and weakened combustion. The mean temperature in Fig. 10 (a) evidenced that heat accumulation occurred at the lower surface. The intumescent coating, which hindered the propagation of the hot flow underneath, resulted in a build-up of hot flow before the coated region. Although fire did not spread further on the lower surface (as evidenced by comparing different times in Fig. 10 (a)) due to the lack of preheating and the limited pyrolysis length, the heat accumulation resulted in a relatively high temperature at the bottom surface.

Conversely, Fig. 10 (b) shows fire spreading across the entire side surface (upper and lower) of the top-coated sample. The pyrolysis length increased proportionally from 20 s to 60 s. It is worth noting that the pyrolysis length was longer at lower surface (x = 0 – 4.5 mm) compared with the upper surface (x = 4.5 – 9.5 mm), indicating that pyrolysis at the lower surface dominated the fire spread. The underlying hot flow persistently preheated the virgin timber, thus propagating the fire. Concurrently, heat was transferred upwards by convection, engaging more materials in pyrolysis. The mean temperature provided further evidence that the lower surface had a higher temperature than the upper surface, with the temperature increasing over time due to the larger pyrolysis area enhancing the combustion.

The bottom surface has been quantitatively proved to be the most effective coating surface compared to other single surfaces. To further investigate the effectiveness of the fire-retardant, the pyrolysis length and mean temperature of bottom-coated samples were compared across different inclined angles, as shown in Fig. 10 (c). The pyrolysis length was found to increase proportionally with the sample inclination due to the larger area was covered by the effective convection heating. Heat accumulation was observed on both the bottom and top surface for all three inclined angles. The mechanisms of the fire-retardant of different coating strategies will be discussed in detail in the following section.

3.4. Surface topography

The quantitative results provided evidence that the different coating strategies can significantly influence the effectiveness of IFR coating, with the bottom surface identified as the most effective single coating surface. In order to reveal the mechanisms of how the coating location influenced the fire-retardant effectiveness, it's essential to explore the mechanisms of intumescent coating. Natural timber materials predominantly comprise of cellulose, hemicellulose and lignin which are biologic polysaccharide [41]. They undergo thermal pyrolysis when they reach a certain temperature, leading to the decomposition and generation of complex products [42] further initiating the flaming combustion and preheating of virgin timber. Fig. 11 shows the SEM images of the timber sample post-burning, both with and without IFR coating. As observed in Fig. 11 (a) and (c), there are discernible cracks and porous features on the timber surface. The combustible gases produced during pyrolysis escape from the timber through these porous structures, forming a hot flow layer in conjunction with the burnt gases, as illustrated in Fig. 8. The porous structure is a crucial factor that the timber can sustain the flaming combustion and the porosity indirectly determined the burning rate of the timber [43].

The intumescent coating is known to swell up to 100 times its original thickness when subjected to fire [44]. This swelling forms a dense layer that covers both the timber surface and the porous structures, as shown in Fig. 11 (b) and (d). The mechanism by which the IFR coating impeded the propagation of the underlying hot gas flow, thereby

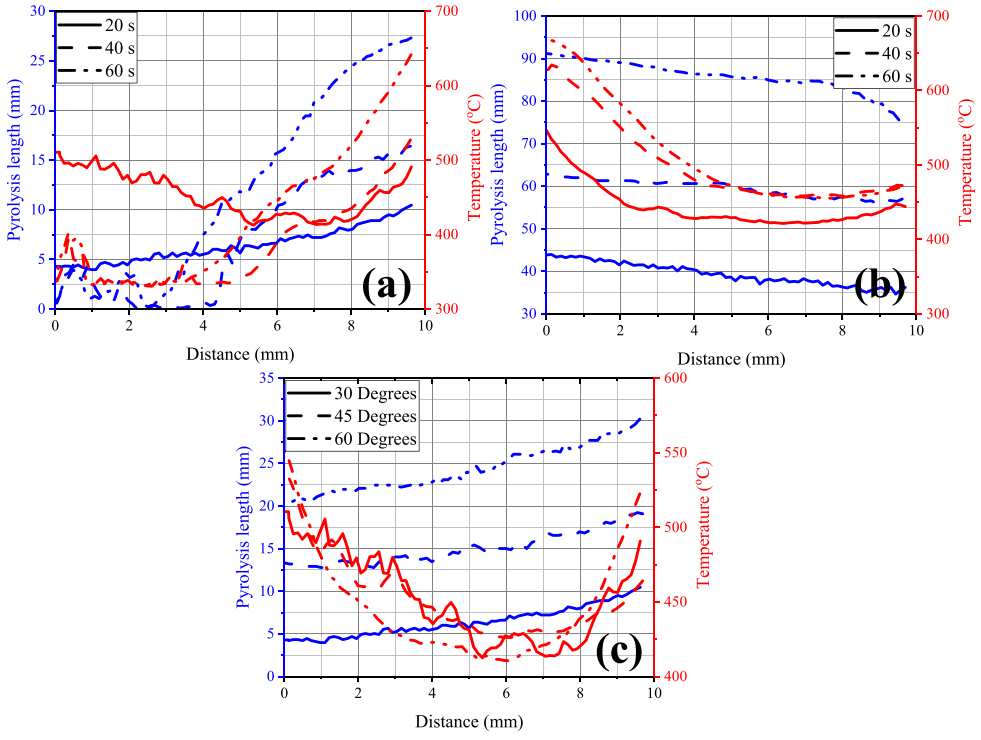

Fig. 10. Side surface pyrolysis length (T > 300 °C) and the average temperature of the pyrolysis region as a function of the distance to the bottom of the sample (demonstrated in Fig. 3 (b)). (a) Bottom surface coated sample inclined at 30 degrees. (b) Top surface coated sample inclined at 30 degrees. And (c) Bottom surface coated sample at different inclination angles (t = 20 s).

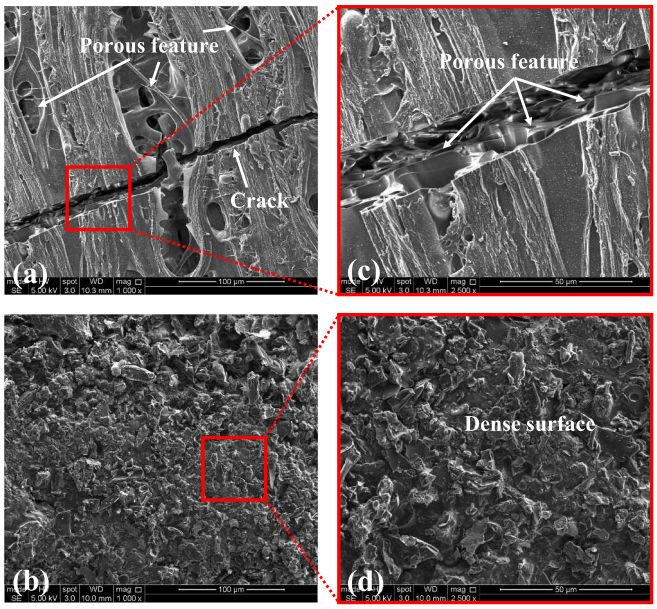

Fig. 11. The SEM images. (a): Uncoated surface ((c): zoomed in region.) (b): Coated surface ((d): zoomed in region).

inhibiting fire spread, can be elucidated based on these SEM images. The intumescent coating provided two critical effects for the fire inhibition. Firstly, the non-combustible coating material prevented the flame propagation by disrupting the supply of oxygen. Consequently, there were no gas-phase products contributed to the hot gas layer. Secondly, the SEM images show that the dense coating layer covered the porous wooden surface. This isolation limited the escape of flammable gases generated from pyrolysis, further diminishing the likelihood of flaming combustion.

3.5. Conceptual models

The fire spread on a timber structure required considerable amount of heat for preheating the virgin wood [24]. Specifically, the fire spread on an individual element of the timber structure (such as beams, columns and frames) relates to the heat transfer in self-sustained burning, as illustrated in Fig. 12 (a). The primary modes of heat transfer are: 1) the radiation emitted from flaming combustion at the top surface. 2) thermal conduction within the timber material, and 3) convective heat transfer from hot gas flow underneath the structure. Timber possesses a low thermal conductivity [35], leading to limited heat transfer within the material. The radiative heat flux relies on the flame temperature [45], the length of flame attachment, and the view factor [32], which can deliver substantial amount of heat to preheat the upper side surface. However, due to the low conductivity of timber materials, the lower surface cannot be effectively preheated, especially when an individual

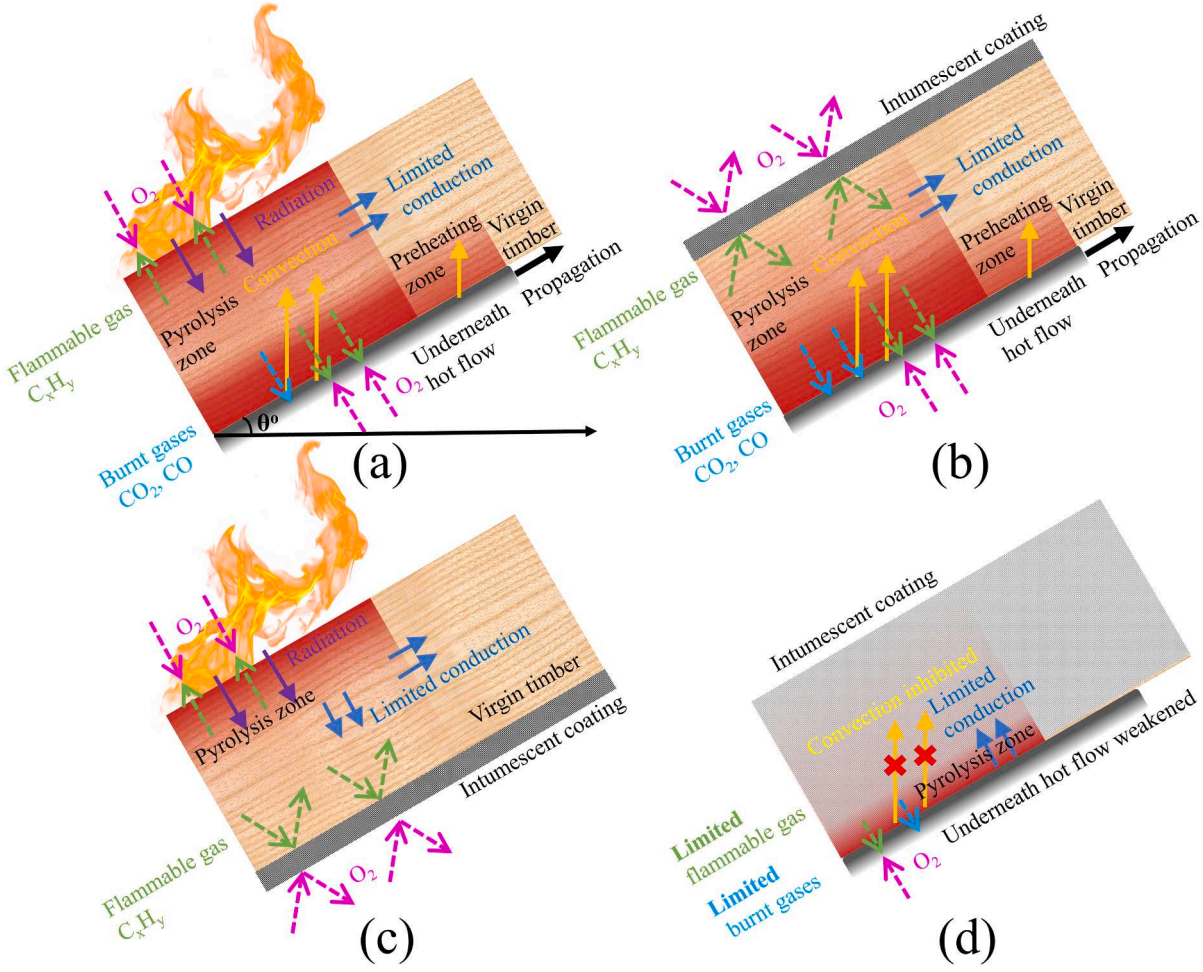

Fig. 12. Conceptual models of fire spread on (a) uncoated wood, (b) top coated wood (c) bottom coated wood and (d) both sides coated wood.

building element has a significant geometrical thickness. Previous research has demonstrated that the convective heat transfer from beneath the timber plays a pivotal role in fire spread on individual elements [24,26,34]. As discussed previously, the underneath hot gas flow consisted of the burnt gases from gas-phase combustion and flammable gases generated from the thermal pyrolysis. This flow heated the upper materials because of the buoyancy and further preheated the virgin timber, thus propagating the fire [31]. Burning can become self-sustained when more regions are involved in pyrolysis, leading to more hot gases being replenished underneath because of the Coanda effect [46]. The visualisation in Fig. 8 directly demonstrated that the surface temperature of the timber samples was strongly correlated with the hot gas flow underneath.

This research explored three different strategies for impeding heat transfer to further inhibit fire spread. These strategies included applying an intumescent coating to the top surface (which inhibited flame radiation, as shown in Fig. 12(b)), the bottom surface (which inhibited convection from underneath, as shown in Fig. 12 (c)), and the side/both sides surfaces (which impeded heat transfer from underneath, as shown in Fig. 12 (d)).

In detail, the flaming combustion on the topside was inhibited when the IFR coating was applied on the top surface. The coating formed a non-combustible layer, preventing the diffusive motions between the gas-phase fuel and the oxidiser. This led to less preheating on the upper surface, which was quantified by the surface temperature in Fig. 10 (b) as the occurrence of heat accumulation near the lower surface. Nevertheless, the hot gas flow underneath continued to heat the material through natural convection, thereby sustaining the fire.

Fig. 12 (c) illustrates the fire spread on a sample with an intumescent coating applied to the bottom surface. The coating prevented the formation of the underneath hot gas layer by inhibiting the escape of gas-phase fuel from the timber and stopping the attachment of burnt gases on the bottom surface. This phenomenon can be observed from the Schlieren images in Fig. 8. The materials at the lower surface cannot be heated effectively (Fig. 10 (a)) because of the low thermal conductivity of timber. Consequently, the heat accumulated near the upper surface, reducing the volume of timber materials that takes part in the pyrolysis process, which resulted in a shorter self-sustained burning lifetime.

Inhibiting convection during its transfer process was another approach to enhance the effectiveness of fire-retardant. The convection was weakened when only one side surface was coated, even though the heat could still pass through the uncoated surface. However, when both side surfaces were coated, as illustrated in Fig. 12 (d), the IFR coating impeded the heat from the underneath convection, resulting in only a limited amount of timber materials being heated by the thermal conduction. This significant reduction in heating led to a marked decrease in the replenishment of gas-phase products towards the underneath hot flow layer. The resulted weakened layer further decreased the provided heat flux, leading to the eventual cessation of the fire.

Increasing the inclination angle can reduce the effectiveness of the fire-retardant coating, as demonstrated by the quantitative results in this study. Fig. 13 illustrates the effects of inclined angles on the convective heat transfer. Heat spontaneously transfers upward by the convective flow because of the buoyancy [32]. Convective preheating can be more effective and cover a larger area of the timber materials with the increasing inclination. This resulted in a larger volume of materials undergoing thermal pyrolysis, leading to a more abundant replenishment of hot gas flow underneath, which in turn preheated a longer length of virgin timber.

The enhanced convective preheating at larger inclined angles caused the top coating and one-side coating to lose their efficiency, as shown in Fig. 9 (b) and (c). This loss of efficiency was attributed to the high-efficiency convection due to geometric factors counteracting the inhibition of the top (radiation) and one side (partly impeded convection), thereby heating the upper surface of the timber. Contrarily, bottom and both-sides coatings impeded and weakened the propagation of the

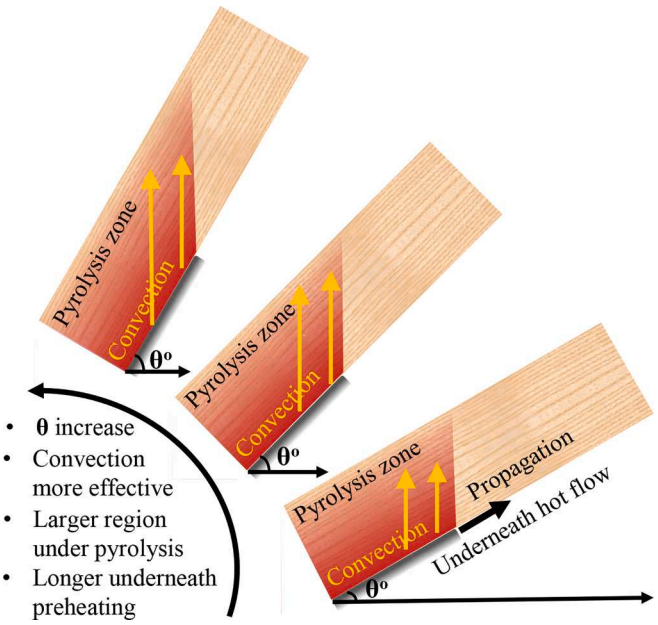

Fig. 13. Effects of inclined angles on the convective heat transfer and the fire spread.

underneath flow, fundamentally inhibiting convection. This explained the remarkable and consistent effectiveness of these two coating strategies regardless of the changes in inclinations.

4. Conclusions

The effects of application locations of intumescent fire-retardant (IFR) coating on the burning behaviours of inclined timber samples were investigated visually and quantitatively using multiple imaging systems and a weight scale. Additionally, the microstructure of the coated surfaces was analysed by a scanning electron microscope (SEM) to investigate the effect on the gas-phase products escape. It was found that the different coating locations strongly influenced the effectiveness of the fire-retardant, which was primarily caused by different methods of the heat transfer inhibition. The fundamental mechanisms were revealed from the results and conceptual models were developed accordingly. Based on the findings of this study, the following conclusions were drawn:

1. IFR coating applied on the bottom surface and both side surfaces of the timber sample proved to be the most effective strategies for mitigating fire spread.
2. The effectiveness of the intumescent coating diminished with larger inclined angles. Specifically, the top and one side coating strategies lost efficiency when the inclined angle exceeded 45°.
3. Convective heat transfer from underneath hot gas flow was considered as the most effective approach of preheating the virgin timber and sustaining burning in a single element structure.
4. The intumescent coating covered the porous structures on the timber materials, preventing the escape of flammable gases generated from thermal pyrolysis, thereby inhibiting combustion reactions.
5. Different coating strategies played unique roles in inhibiting heat transfer:

- Bottom coating impeded convection by cutting off the hot gas flow from underneath.
- Top coating prevented gas-phase combustion on the top surface, inhibiting radiation emitted from the flame.
- Side coating (single side and both sides) partially or fully impeded convection along its transfer path.

The insights from this work hold significant importance as they provide both theoretical and practical guidance for enhancing fire safety in timber-based construction. While the results provide new insights into heat transfer mechanisms and the role of coating locations, they are based on small-scale samples. In future research, the insights gained from this study will be utilised to design and conduct full-scale experiments, thereby extending the applicability and validity of our findings to real-world construction scenarios.

CRediT authorship contribution statement

Yufeng Lai: Writing – review & editing, Writing – original draft, Visualization, Validation, Software, Methodology, Investigation, Formal analysis, Data curation, Conceptualization. **Xuanqi Liu:** Writing – review & editing, Validation, Methodology, Investigation, Data curation, Conceptualization. **Yifan Li:** Writing – review & editing, Validation, Formal analysis, Data curation, Conceptualization. **Emilios Leonidas:** Writing – review & editing, Validation, Investigation. **Callum Fisk:** Writing – review & editing, Investigation, Conceptualization. **Jiansheng Yang:** Writing – review & editing, Validation, Methodology. **Yang Zhang:** Writing – review & editing, Supervision, Resources, Conceptualization. **Jon Willmott:** Writing – review & editing, Supervision, Software, Resources, Project administration, Investigation, Conceptualization.

Declaration of Competing Interest

The authors declare that they have no known competing financial interests or personal relationships that could have appeared to influence the work reported in this paper.

Data availability

Data will be made available on request.

References

[1] F.M. Amoruso, T. Schuetze, Life cycle assessment and costing of carbon neutral hybrid-timber building renovation systems: Three applications in the Republic of Korea, Build. Environ. 222 (Aug. 2022), https://doi.org/10.1016/j.buildenv.2022.109395.

[2] J.H. Andersen, N.L. Rasmussen, M.W. Ryberg, Comparative life cycle assessment of cross laminated timber building and concrete building with special focus on biogenic carbon, Energ. Buildings 254 (Jan. 2022), https://doi.org/10.1016/j.enbuild.2021.111604.

[3] W. Hawkins, S. Cooper, S. Allen, J. Roynon, T. Ibell, Embodied carbon assessment using a dynamic climate model: Case-study comparison of a concrete, steel and timber building structure, Structures 33 (Oct. 2021) 90–98, https://doi.org/10.1016/j.istruc.2020.12.013.

[4] J.M. Khatib, Sustainability of construction materials, Woodhead Pub, 2008.

[5] M.I. Shahidul, M.L. Malcolm, M.S.J. Hashmi, M.H. Alhaji, Waste Resources Recycling in Achieving Economic and Environmental Sustainability: Review on Wood Waste Industry, in: S. Hashmi, I.A. Choudhury (Eds.), Encyclopedia of Renewable and Sustainable Materials, Elsevier, Oxford, 2020, pp. 965–974, https://doi.org/10.1016/B978-0-12-803581-8.11275-5.

[6] R. Duriot, F.J. Rescalvo, G. Pot, L. Denaud, S. Girardon, R. Frayssinhes, An insight into mechanical properties of heartwood and sapwood of large French Douglas-fir LVL, Constr. Build. Mater. 299 (2021), 123859, https://doi.org/10.1016/j.conbuildmat.2021.123859.

[7] P. Moradpour, H. Pirayesh, M. Gerami, I. Rashidi Jouybari, Laminated strand lumber (LSL) reinforced by GFRP; mechanical and physical properties, Constr. Build. Mater. 158 (2018) 236–242, https://doi.org/10.1016/j.conbuildmat.2017.09.172.

[8] R. Brandner, G. Flatscher, A. Ringhofer, G. Schickhofer, A. Thiel, Cross laminated timber (CLT): overview and development, Eur. J. Wood Wood Prod. 74 (3) (2016) 331–351, https://doi.org/10.1007/s00107-015-0999-5.

[9] D. Barber, Determination of fire resistance ratings for glulam connectors within US high rise timber buildings, Fire Saf. J. 91 (2017) 579–585, https://doi.org/10.1016/j.firesaf.2017.04.028.

[10] B. Chorlton, J. Gales, Mechanical performance of laminated veneer lumber and Glulam beams after short-term incident heat exposure, Constr. Build. Mater. 263 (2020), 120129, https://doi.org/10.1016/j.conbuildmat.2020.120129.

[11] 'BS EN 1995-1-2:2004 Eurocode 5: Design of timber structures. General - Structural fire design (incorporating corrigenda June 2006 and March 2009)', 2004.

[12] J. Liblik, M. Nurk, A. Just, Charring performance of timber structures protected by traditional lime-based plasters, Constr. Build. Mater. 347 (2022), 128572, https://doi.org/10.1016/j.conbuildmat.2022.128572.

[13] C. Gorska, J.P. Hidalgo, J.L. Torero, Fire dynamics in mass timber compartments, Fire Saf. J. 120 (2021), 103098, https://doi.org/10.1016/j.firesaf.2020.103098.

[14] H. Xu, et al., Large-scale compartment fires to develop a self-extinction design framework for mass timber—Part 1: Literature review and methodology, Fire Saf. J. 128 (2022), 103523, https://doi.org/10.1016/j.firesaf.2022.103523.

[15] R.G. Puri, A.S. Khanna, Intumescent coatings: A review on recent progress, J. Coat. Technol. Res. 14 (1) (2017) 1–20, https://doi.org/10.1007/s11998-016-9815-3.

[16] A. Lucherini, Q.S. Razzaque, C. Maluk, Exploring the fire behaviour of thin intumescent coatings used on timber, Fire Saf. J. 109 (2019), 102887, https://doi.org/10.1016/j.firesaf.2019.102887.

[17] J. Jiang, J. Li, J. Hu, D. Fan, Effect of nitrogen phosphorus flame retardants on thermal degradation of wood, Constr. Build. Mater. 24 (12) (2010) 2633–2637, https://doi.org/10.1016/j.conbuildmat.2010.04.064.

[18] Y. Wang, J. Zhao, Preliminary study on decanoic/palmitic eutectic mixture modified silica fume geopolymer-based coating for flame retardant plywood, Constr. Build. Mater. 189 (2018) 1–7, https://doi.org/10.1016/j.conbuildmat.2018.08.205.

[19] Y. Wang, J. Zhao, Benign design of intumescent flame retardant coating incorporated various carbon sources, Constr. Build. Mater. 236 (2020), 117433, https://doi.org/10.1016/j.conbuildmat.2019.117433.

[20] F. Song, et al., Sustainable, high-performance, flame-retardant waterborne wood coatings via phytic acid based green curing agent for melamine-urea-formaldehyde resin, Prog. Org. Coat. 162 (2022), 106597, https://doi.org/10.1016/j.porgcoat.2021.106597.

[21] Y. Wang, K. Yu, J. Zhao, A. Xin, NaOH hydrothermally treated gibbsite modified silicone acrylic emulsion-based intumescent flame-retardant coatings for plywood, Colloids Surf. A Physicochem. Eng. Asp 646 (2022), 129001, https://doi.org/10.1016/j.colsurfa.2022.129001.

[22] X. Hu, Z. Sun, Nano CaAlCO3-layered double hydroxide-doped intumescent fire-retardant coating for mitigating wood fire hazards, J. Build. Eng. 44 (2021), 102987, https://doi.org/10.1016/j.jobe.2021.102987.

[23] Y. Zhang, X. Yang, Y. Luo, Y. Gao, H. Liu, T. Li, Experimental study of compartment fire development and ejected flame thermal behavior for a large-scale light timber frame construction, Case Stud. Therm. Eng. 27 (2021), 101133, https://doi.org/10.1016/j.csite.2021.101133.

[24] Y. Lai, X. Wang, T.B.O. Rockett, J.R. Willmott, H. Zhou, Y. Zhang, The effect of preheating on fire propagation on inclined wood by multi-spectrum and schlieren visualisation, Fire Saf. J. 118 (2020), https://doi.org/10.1016/j.firesaf.2020.103223.

[25] G. Di Cristina, N.S. Skowronski, A. Simeoni, A.S. Rangwala, S.K. Im, Flame spread behavior characterization of discrete fuel array under a forced flow, Proc. Combust. Inst. 38 (3) (2021) 5109–5117, https://doi.org/10.1016/j.proci.2020.05.035.

[26] Y. Lai, et al., Investigation of forced flow orientations on the burning behaviours of wooden rods using a synchronised multi-imaging system, Proc. Combust. Inst. (2022), https://doi.org/10.1016/j.proci.2022.07.057.

[27] Y. Wu, H. J. Xing, and G. Atkinson, 'Interaction of "re plume with inclined surface', 2000.

[28] K. Wang, et al., Influence of air gap ratio of the Chinese historical wooden window on the vertical flame spread performance, Therm. Sci. Eng. Progr. 32 (Jul. 2022), https://doi.org/10.1016/j.tsep.2022.101308.

[29] Y. Lai, et al., Combustion inhibition of biomass charcoal using slaked lime and dolime slurries, Fire Saf. J. (Jun. 2023), 103841, https://doi.org/10.1016/j.firesaf.2023.103841.

[30] M.J. DiDomizio, P. Mulherin, E.J. Weckman, Ignition of wood under time-varying radiant exposures, Fire Saf. J. 82 (May 2016) 131–144, https://doi.org/10.1016/j.firesaf.2016.02.002.

[31] Y. Lai, X. Wang, T.B.O. Rockett, J.R. Willmott, Y. Zhang, Investigation into wind effects on fire spread on inclined wooden rods by multi-spectrum and schlieren imaging, Fire Saf. J. 127 (July) (2021) 103513, https://doi.org/10.1016/j.firesaf.2021.103513.

[32] D. Drysdale, An introduction to fire dynamics, John Wiley & Sons, 2011.

[33] M.J. Gollner, X. Huang, J. Cobian, A.S. Rangwala, F.A. Williams, Experimental study of upward flame spread of an inclined fuel surface, Proc. Combust. Inst. 34 (2) (2013) 2531–2538, https://doi.org/10.1016/j.proci.2012.06.063.

[34] R.O. Weber, N.J. De Mestre, Flame Spread Measurements on Single Ponderosa Pine Needles: Effect of Sample Orientation and Concurrent External Flow, Combust. Sci. Technol. 70 (1–3) (1990) 17–32, https://doi.org/10.1080/00102209008951609.

[35] S.J. Chang, S. Wi, S. Kim, Thermal bridging analysis of connections in cross-laminated timber buildings based on ISO 10211, Constr. Build. Mater. 213 (Jul. 2019) 709–722, https://doi.org/10.1016/j.conbuildmat.2019.04.009.

[36] H. Hao, C.L. Chow, D. Lau, Effect of heat flux on combustion of different wood species, Fuel 278 (Oct. 2020), https://doi.org/10.1016/j.fuel.2020.118325.

[37] V. Babrauskas, Ignition of wood: A review of the state of the art, J. Fire. Prot. Eng. 12 (3) (2002) 163–189, https://doi.org/10.1177/10423910260620482.

[38] M. A. Dietenberger and L. E. Hasburgh, 'Wood Products: Thermal Degradation and Fire', in *Reference Module in Materials Science and Materials Engineering*, Elsevier, 2016. doi: 10.1016/b978-0-12-803581-8.03338-5.

[39] Z. Xin, et al., Assessing the density and mechanical properties of ancient timber members based on the active infrared thermography, Constr. Build. Mater. 304 (Oct. 2021), https://doi.org/10.1016/j.conbuildmat.2021.124614.

[40] J. ichi Suzuki, T. Mizukami, T. Naruse, and Y. Araki, 'Fire Resistance of Timber Panel Structures Under Standard Fire Exposure', *Fire Technol*, vol. 52, no. 4, pp. 1015–1034, Jul. 2016, doi: 10.1007/s10694-016-0578-2.
[41] A.I. Bartlett, R.M. Hadden, L.A. Bisby, A Review of Factors Affecting the Burning Behaviour of Wood for Application to Tall Timber Construction, Fire Technol. 55 (1) (2019) 1–49, https://doi.org/10.1007/s10694-018-0787-y.
[42] T.T. Tran, et al., Fire structural performance of thermo-mechanically compressed spruce timber by means experiments and a three-step multi-reactions pyrolysis 3D-finite element modelling, Constr. Build. Mater. 320 (Feb. 2022), https://doi.org/10.1016/j.conbuildmat.2021.126100.
[43] Q. Wang, K. Liu, S. Wang, Effect of porosity on ignition and burning behavior of cellulose materials, Fuel 322 (Aug. 2022), https://doi.org/10.1016/j.fuel.2022.124158.
[44] R.G. Puri, A.S. Khanna, Intumescent coatings: A review on recent progress, J. Coat. Technol. Res. 14 (1) (Jan. 2017) 1–20, https://doi.org/10.1007/s11998-016-9815-3.
[45] R. Viskanta and M. P. Mengoqt, 'Radiation heat transfer in combustion systems', 1987.
[46] D.J. Tritton, Physical fluid dynamics, Springer Science & Business Media, 2012.